Research Square

Preprints are preliminary reports that have not undergone peer review.
They should not be considered conclusive, used to inform clinical practice,
or referenced by the media as validated information.

Differential Susceptibility of Salmonella enterica Serotypes to Antimicrobial Photodynamic Therapy: From Planktonic Eradication to Biofilm Recalcitrance

Florencia Amancay Colocho

florenciacolocho@gmail.com

Instituto Multidisciplinario de Investigaciones Biológicas de San Luis-Consejo Nacional de Investigaciones Científicas y Técnicas (IMIBIO-SL-CONICET)

Juan Eduardo Silva

Instituto Multidisciplinario de Investigaciones Biológicas de San Luis-Consejo Nacional de Investigaciones Científicas y Técnicas (IMIBIO-SL-CONICET)

Francisca Ailín Rocca Plaza

National University of San Luis

Gabriela Isabel Favier

National University of San Luis

Carlos Rodolfo Pungitore

Instituto Instituto de Investigación en Tecnología Química (INTEQUI-SL-CONICET)

Cecilia Stella Marys Lucero Estrada

Instituto Multidisciplinario de Investigaciones Biológicas de San Luis-Consejo Nacional de Investigaciones Científicas y Técnicas (IMIBIO-SL-CONICET)

Research Article

Keywords: Biofilm, Cationic porphyrins, Photodynamic inactivation, Salmonella enterica

Posted Date: August 3rd, 2026

DOI: https://doi.org/10.21203/rs.3.rs-10474596/v1

License: This work is licensed under a Creative Commons Attribution 4.0 International License.
Read Full License

Additional Declarations: No competing interests reported.

Abstract

This study systematically optimized biofilm cultivation conditions (media and incubation time) for fifteen *Salmonella enterica* strains, selecting one representative of each serovar for comparative evaluation. Under these optimized parameters and defined light fluence as 13.19 J/cm^2, the antimicrobial and antibiofilm activities of seven porphyrin and phthalocyanine compounds were screened, identifying 5,10,15,20-Tetrakis(1-methyl-4-pyridinio) porphyrin tetra (p-toluenesulfonate) (**C7**) as the most efficacious photosensitizer. In planktonic cultures, **C7**-mediated antimicrobial photodynamic therapy (aPDT) achieved minimum inhibitory concentration (MIC) at 6.25 μM, reaching a 3.00 $\log_{10}$ reduction (99.9% lethality) at 2 h post-irradiation. On the other hand, at sub-inhibitory conditions 1.56 μM (1/4 MIC), aPDT induced an immediate bacterial load reduction of 2.87 and 2.31 $\log_{10}$ for strains S4 (*S.* Enteritidis) and SB3 (*S.* Typhimurium) respectively, and this same effect was observed using flow cytometry; however, longitudinal kinetics revealed a prominent phenotypic regrowth within 24 h driven by a resilient subpopulation. Notably, at the same concentration, **C7** effectively prevented biofilm development, significantly reducing exopolysaccharides (EPS) production and altering macrocolony morphotypes, which indicates impairment in curli fimbriae and matrix synthesis. Upon encountering mature biofilms, a striking divergence in susceptibility emerged: strain SB3 exhibited marked recalcitrance compared to strain S4. This highlights that serotype-specific macrocolony architecture and defensive matrix over-fortification in biofilm, play a protective role that supersedes individual cell envelope robustness. Overall, while aPDT represents an excellent alternative for planktonic eradication and biofilm prevention, eliminating established mature biofilms in strong biofilm-forming strains remains a significant challenge.

Introduction

The genus *Salmonella* is divided into two main species, *Salmonella enterica* and *Salmonella bongori*, with the former being of greater clinical relevance. *S. enterica* is further subdivided into more than 2,600 serotypes, among which *S.* Typhimurium and *S.* Enteritidis are the most frequently identified in the food industry and the primary cause of salmonellosis outbreaks worldwide (Mkangara 2023). As a major zoonotic pathogen, it represents the third leading cause of mortality associated with foodborne diarrheal diseases globally. The persistence of this microorganism in the food production chain, particularly within the poultry industry, is mainly attributed to its ability to form biofilms on biotic and abiotic surfaces (Pang et al. 2023). The establishment of these sessile communities confers inherent tolerance to environmental stress conditions and the action of disinfectant agents, exacerbated by an extracellular polymeric substance (EPS) matrix that acts as a diffusional and protective barrier (Gentile et al. 2025). Extracellular matrix production is coordinated by the master regulator *csgD*, which activates the expression of key genes such as *csgA* (responsible for curli fimbriae) and *adrA* or *bcsA* (involved in cellulose synthesis), fundamental components for the structural stability of the biofilm (Chen et al. 2021).

The eradication of *Salmonella* presents an additional challenge due to the complex architecture of its Gram negative cell envelope. The outer membrane functions as a selective permeability barrier that

limits the uptake of anionic or neutral antimicrobial agents, hindering the efficacy of conventional treatments (Breijyeh et al. 2020). Given the global emergence of multidrug-resistant strains and the ineffectiveness of traditional sanitization protocols, the implementation of unconventional strategies is required (Soares et al. 2025). In this context, Antimicrobial Photodynamic Therapy (aPDT) has emerged as a promising alternative; this approach is primarily based on the extracellular generation of Reactive Oxygen Species (ROS) within the bacterial microenvironment, triggered by the light activation of a photosensitizer (Shariati et al. 2022).

Although aPDT has demonstrated high efficacy against Gram positive bacteria, its application in Gram negatives requires the use of photosensitizers designed to overcome the outer membrane barrier. Cationic porphyrins have shown superior electrostatic interaction with the anionic components of the lipopolysaccharide (LPS), facilitating cell binding and penetration (Reynoso et al. 2019). Porphyrins photoactivation induces lethal damage in bacteria through the production of singlet oxygen and free radicals, affecting multiple molecular targets, including membrane integrity, cytosolic proteins, and genomic DNA (Mamone et al. 2024).

In addition to its direct bactericidal action, aPDT offers significant advantages, such as a low risk of inducing bacterial resistance following sub-lethal exposures (Cassidy et al. 2010) and the ability to disrupt the structure of mature biofilms (Mamone et al. 2024). Despite these advances, there is a knowledge gap regarding the physiological and molecular response of *Salmonella* to photodynamic therapy. The present study aims to evaluate the efficacy of porphyrin and phthalocyanine derivatives in aPDT on the planktonic and biofilm growth of *Salmonella* sp, analysing cellular damage mechanisms and the modulation of virulence factors.

Materials and Methods

Bacterial strains and culture conditions

A panel of 15 clinical strains of *Salmonella* enterica was used, belonging to the serotypes Typhimurium, Enteritidis, and Montevideo, previously isolated and biochemically characterized in our laboratory (Table 1). Stock cultures were preserved in Luria Bertani Broth (LBB Britania, Buenos Aires, Argentina) added with 20% glycerol at -80°C. For experimental use, bacteria were reactivated in Tryptic Soy Broth (TSB; Britania) and incubated aerobically at 37°C until reaching the stationary phase. Subsequently, the inocula were adjusted to the required optical density via spectrophotometry according to the specific requirements of each assay.

Table 1
Capacity to form biofilm of 15 *Salmonella* sp strains in three different media.

Number collection	Serotype	Culture medium*		
		LB	TSB	TSBG
59	*S.* Montevideo	SBF	SBF	MBF
SB1	*S.* Typhimurium	MBF	SBF	MBF
SB2	*S.* Typhimurium	WBF	MBF	MBF
SB3	*S.* Typhimurium	SBF	SBF	SBF
ST1	*S.* Typhimurium	MBF	SBF	MBF
ST2	*S.* Typhimurium	WBF	MBF	MBF
S2	*S.* Enteritidis	MBF	MBF	MBF
S3	*S.* Enteritidis	MBF	MBF	SBF
S4	*S.* Enteritidis	MBF	SBF	MBF
S21	*S.* Enteritidis	MBF	MBF	MBF
S90	*S.* Enteritidis	WBF	MBF	WBF
S106	*S.* Enteritidis	WBF	SBF	WBF
S107	*S.* Enteritidis	MBF	MBF	WBF
S112	*S.* Enteritidis	MBF	SBF	WBF
S113	*S.* Enteritidis	MBF	MBF	WBF

*Strains were categorized as Weak (WBF), Moderate (MBF), or Strong (SBF) biofilm formers following the criteria of Santos et al. (2022). Evaluation was performed in LB (Luria Bertani broth); TSB (Tryptic Soy Broth and TSBG (TSB added with 0.5% w/v glucose) after 24 h of incubation.

Photosensitizers and irradiation conditions

Seven commercially acquired synthetic porphyrin and phthalocyanine derivatives (Sigma-Aldrich, St. Louis, MO, USA) were evaluated (Fig. 1). Stock solutions were prepared in dimethyl sulfoxide (DMSO analytical grade, > 99.9%; Sistemas Analíticos, Argentina) at a concentration of 10 mM and stored in the dark at 4°C. In all assays, the final concentration of DMSO was kept below 5% (v/v) to avoid intrinsic vehicle toxicity (Di Marco et al. 2019). A white light LED system (50W; Philips, Argentina) positioned seven centimetres from the sample was used as the irradiation source. The illuminance at the irradiation surface was 5500 lux, quantified by a luxmeter (model MLX-1011; Gralf, Argentina), equivalent to an irradiance of 1.83 mW/cm².

Selection of the optimal medium for biofilm formation and biofilm growth kinetics

To identify the nutritional conditions favouring the highest production of sessile biomass, a screening assay was performed using three culture media with increasing concentrations of glucose: LBB, (sugar-free); TSB (0.25% w/v glucose); and supplemented TSB (TSBG; 0.5% w/v glucose). Flat 96-well polystyrene plates (Delta-lab, Barcelona, Spain) were inoculated with a bacterial suspension adjusted to $1x10^7$ CFU/mL in each evaluated medium. After 24 h of static incubation at 37°C, the quantification of the biofilm was performed using the crystal violet (CV) staining technique according to Di Marco et al. (2025), measuring absorbance at 570 nm in a microplate reader (Epoch Microplate Spectrophotometer, Bioteck Instrument, Winooski, USA).

For biofilm growth kinetics, inoculum of $1x10^7$ CFU/mL in TSB were prepared and incubated in flat 96-well plates at 37°C. Biomass formation was quantified using the CV technique at defined time intervals: 2, 4, 6, 8, 24, 48, and 72 hours.

Antibacterial activity

The ability of the porphyrins to inhibit planktonic bacterial growth was determined using a modified Kirby-Bauer method. Mueller-Hinton agar plates (MHB, Britania) were inoculated with a standardized bacterial suspension at $1x10^8$ CFU/mL. Subsequently, 2 µL aliquots of the photosensitizers at a concentration of 10 mM were deposited onto the agar. Activity was evaluated by comparing two conditions: darkness (control) and white light irradiation at increasing times until reaching a maximum fluence of 32.99 J/cm², corresponding to 5 h. Gentamicin was used as a positive inhibition control (darkness) and DMSO as a negative control for solvent toxicity.

Minimum Inhibitory Concentration (MIC) and Minimum Bactericidal Concentration (MBC) were determined using the broth microdilution method according to the Clinical and Laboratory Standards Institute (2024), adapted to 24-well plates. A bacterial inoculum adjusted to $5x10^5$ CFU/mL in MHB and TSB was prepared. Serial two-fold dilutions of the compounds were performed starting from 100 µM in a final volume of 300 µL in polystyrene 24-well plates (Delta-lab). Plates were irradiated under the standardized condition obtained as mentioned above and incubated at 37°C for 24 h. MIC was defined as the lowest concentration of the compound capable of inhibiting visible bacterial growth. To determine MBC, aliquots from wells without turbidity were seeded on nutrient agar (NA; Britania) plates using the drop plate method. After 24 h of incubation, MBC was determined as the minimum concentration capable of eradicating 99.9% of the initial inoculum.

Survival curves

After overnight growth in TSB, a bacterial suspension of each *Salmonella* strain was prepared and adjusted to a final concentration of 1x10⁶ CFU/mL. A final volume of 2 mL of these suspensions was transferred into 35 mm diameter Petri dishes. The use of small Petri dishes instead of flasks was specifically chosen to guarantee a minimal optical path length and uniform light penetration across the entire sample, ensuring experimental reproducibility. The samples were divided into four experimental conditions: a growth control (without photosensitizer) and treatments supplemented with the chosen photosensitizer at concentrations corresponding to ¼ MIC, MIC, and 4 MIC. The plates were incubated at 37°C. To evaluate the bacterial death kinetics, 10 µL aliquots were collected at specific time points: during the pre-irradiation period (-2 h and – 1 h) and at different post-treatment times (0, 1, 2, 3, 4, and 24 h). Small aliquot volumes were extracted to ensure that the overall final volume and bacterial growth dynamics remained unaltered throughout the assay. At each time point, samples were serially diluted in TSB and plated in triplicate using the drop plate method for viable cell counting.

Planktonic viability evaluation

The metabolic activity of treated planktonic cells was evaluated using the 3-(4,5-dimethylthiazol-2-yl)-2,5-diphenyltetrazolium bromide (MTT, Invitrogen, ThermoFisher, USA) reduction assay according to Benov (2019). In 24-well plates, a 5x10⁵ CFU/mL inoculum in TSB was exposed to concentrations of the selected photosensitizer corresponding to ¼ MIC, ½ MIC, and ¾ MIC, alongside a control of the strain without the compound and a broth control without inoculum and compound. After irradiation under the standardized conditions, plates were incubated for 24 h at 37°C, and finally 270 µL of MTT solution (5 mg/mL) was added and incubated for 30 min at 37°C with agitation. The formed formazan crystals were solubilized by adding 10% SDS in 0.01 M HCl, followed by 1 h incubation in the dark. Absorbance was measured at 560 nm (Epoch Microplate Spectrophotometer).

Membrane integrity evaluation by Flow Cytometry

Cytoplasmic membrane damage was evaluated using the LIVE/DEAD BacLight Bacterial Viability kit (Invitrogen, Eugene, OR, USA). Inoculum of $1x10^6$ CFU/mL were treated with the chosen photosensitizer (¼ MIC, MIC, 4 MIC) and irradiated cells were stained the LIVE/DEAD kit for 15 min in the dark. Acquisition was performed on a FACSCalibur, (Becton Dickinson, Mountain View, CA, USA) flow cytometer and analysis was performed using FlowJo, (Tree Star, Ashland, OR, USA) software. Events for 120 s were acquired. Live cell controls (untreated) and dead cell controls (treated with 70% isopropanol) were used to adjust voltages and compensations.

Activity of a photosensitizer on Salmonella spp. Biofilm

Inhibition of biofilm formation and eradication

These techniques were performed according to Di Marco et al. (2025) with some modifications. To evaluate the Biofilm Formation Preventive Concentration (BFPC), bacterial suspensions of $1x10^7$ CFU/mL in TSB were co-incubated with serial two-fold dilutions of the chosen photosensitizer starting from 2 MIC in 24-well plates. After irradiation, they were incubated for 24 h at 37°C, and finally, the adhered biomass was quantified by CV staining. To determine the Minimum Biofilm Eradication Concentration (MBEC), mature biofilms (24 h, 37°C) were formed in the absence of the compound in 24-well plates. After washing the wells with sterile saline phosphate buffer (PBS) to remove planktonic cells, fresh broth with serial two-fold concentrations of the chosen photosensitizer starting at 200 µM (maximum allowed DMSO solvent concentration) was added. The plates were irradiated and incubated for another 24 h. The viability of the remaining biofilm was determined qualitatively by adding TSB broth supplemented with 0.2% 2,3,5-triphenyltetrazolium chloride (TTC; Anedra, Buenos Aires, Argentina). The appearance of a red colour after 6 h indicated respiratory metabolic activity.

Characterization of colony morphotype

To assess the effect of aPDT on the phenotypic expression of extracellular matrix components (curli and cellulose), the macrocolony morphotype technique described by Merritt et al. (2011) with some modifications were performed. Bacterial suspensions of $1x10^8$ CFU/mL were prepared in TSB and placed in a 24-well plate. The cultures were treated with the chosen photosensitizer at concentrations ranging from the MIC to 0.39 µM and subsequently irradiated. This experimental setup was chosen to ensure uniform light distribution and experimental reproducibility, as direct irradiation of the droplet on the agar surface proved inconsistent. After treatment, 4 µL aliquots were collected from each well and seeded onto the surface of Congo Red Agar (CRA; brain heart agar supplemented with 5% w/v sucrose and 0.08% w/v Congo Red) and Tryptic Soya Agar (TSA; TSB with 1.7% w/v agar). After 48 h of incubation at 37°C, the macrocolonies were examined and classified according to RDAR (rough, dry, and red) or PDAR (pink/pale and smooth) morphotypes (Steenackers et al., 2012).

Quantification of exopolysaccharides (EPS)

EPS production in treated biofilms was quantified using of the Congo Red method (Ušjak et al. 2024) with some modifications. The preventive treatment protocol was followed (see 2.8.1). After incubation, biofilms were washed and stained with 300 µL of Congo Red (CR; Merck, Darmstadt, Germany) solution of 1%, p/v for 1 day. The dye adsorbed to the matrix was solubilized with DMSO and absorbance was measured at 490 nm.

Biofilm viability

The metabolic activity of sessile cells was determined via MTT reduction. Biofilms formed and treated according to the preventive protocol were washed twice with PBS. Fresh broth was added, the surface was scraped to release sessile cells, and MTT solution was added; incubation and formazan solubilisation were performed followed the protocol described in section 2.6.

Statistical analysis

Three replications of each experiment were performed on different days. Means of plate counts were analysed for differences in treatment response by analysis of variance and subsequent Dunnet test, using Graph Pad Prism 8 statistical software (GraphPad Software, Boston, MA USA). The confidence limit used was 0.05. *P* values used were: < 0.0001, very highly significant (∗∗∗∗); < 0.001, highly significant (∗∗∗); < 0.01, very significant (∗∗); < 0.05, significant (∗); > 0.05, not significant.

Results

Selection of the optimal medium for biofilm formation and biofilm growth kinetics

The ability of *Salmonella enterica* to persist in industrial and clinical environments is closely linked to its metabolic flexibility and biofilm formation, so the biofilm-forming capacity of 15 *Salmonella* spp. strains was evaluated in three culture media with varying glucose availability (LBB, TSB, and TSBG). Following the classification criteria described by dos Santos et al. (2022), the isolates were categorized as weak, moderate, or strong biofilm formers (WBF, MBF, and SBF, respectively). As shown in Fig. 2.a. and Table 1, sessile biomass production varied significantly depending on the nutritional composition of the medium. TSB (0.25% glucose) was identified as the optimal medium, promoting the most robust phenotype with 46% (seven out of 15) of the strains classified as SBF. Conversely, in LBB (glucose-deficient) and TSBG (0.5% glucose), most isolates exhibited either weak or moderate biofilm-forming capacity. Based on this screening, strains S4 (*S*. Enteritidis) and SB3 (*S.* Typhimurium) were selected for subsequent assays due to their high biomass production in TSB.

To determine the optimal maturation time, the biofilm formation kinetics of strains S4 and SB3 were monitored over 72 hours. Both strains reached peak sessile biomass at 24 h of incubation (Fig. 2b), followed by a progressive decline in biomass production at 48 and 72 hours. Consequently, 24 h was defined as the optimum maturation time for subsequent photodynamic assays, ensuring evaluation at the point of maximum biofilm biomass.

Antibacterial Activity

An initial assessment of the intrinsic toxicity of the seven porphyrin and phthalocyanine derivatives showed that none inhibited bacterial growth in the absence of light stimulation at a concentration of 10 mM. Upon photoactivation, antibacterial activity was observed for Compound 4 (**C4**), Compound 5 (**C5**), and Compound 7 (**C7**) (Supplement Table 1).

To standardize the treatment protocol, the relationship between light exposure time (fluence) and the inhibition halo size was analysed. Antibacterial activity increased proportionally with the light dose up to 2 h of irradiation, corresponding to a fluence of 13.19 J/cm^2. Extending irradiation beyond this point (up to 5 h) resulted in no significant differences in the inhibition diameter ($p > 0.001$), indicating a plateau in

photodynamic efficacy. Consequently, 13.19 J/cm^2 (2 h) was established as the standard light dose for all subsequent experiments (Fig. 2c).

The photodynamic activity of **C4**, **C5**, and **C7** against planktonic cells was quantified by determining their MIC and MBC values in MHB and TSB media (Table 2). The calculated bactericidal index (MBC/MIC) was 1 for all three compounds, confirming potent bactericidal activity. In MHB, **C7** was the most effective, with MIC and MBC values of 12.5 μM for *S.* Typhimurium SB3 strain and 25 μM for *S*. Enteritidis S4 strain; **C4** showed intermediate activity (25 μM for both strains), while **C5** required 50 μM. When evaluated in TSB, bacterial susceptibility increased, with MIC and MBC values decreasing by half compared to MHB. In this medium, **C7** exhibited the highest potency, achieving complete inhibition at 6.25 μM for both strains. Based on these results, **C7** was selected for subsequent biofilm photoinactivation and mechanistic assays.

Survival Curves

The inactivation dynamics and potential for post-treatment recovery were evaluated by monitoring the viability of *S.* Enteritidis S4 and *S.* Typhimurium SB3 over time across different **C7** concentrations. For strain S4 (Fig. 3a), treatment at 4 MIC resulted in an immediate bactericidal effect, with viable counts falling below the detection limit (> 6.00 $\log_{10}$ reduction) at 0 h post-irradiation, with no bacterial recovery observed at 24 h. At the MIC, an initial bacterial load reduction of 2.87 $\log_{10}$ was observed at 0 h, with viability declining further until reaching the detection limit at 2 h post-irradiation, remaining stable thereafter. In contrast, the 1/4 MIC dose induced only transient inhibition, followed by bacterial population recovery.

Strain SB3 exhibited distinct inactivation kinetics (Fig. 3a). Immediately following irradiation (0 h), a 3.00 $\log_{10}$ decrease was observed across all tested concentrations. Treatment at 4 MIC achieved complete inactivation at 3 h post-irradiation, while the MIC required 4 h to reach the same threshold; in both cases, no recovery was observed at 24 h. Conversely, cells treated at 1/4 MIC showed significant resilience, with the population initiating a gradual regrowth process after 0 h, reaching viability levels comparable to the untreated control by the end of the assay.

Planktonic viability evaluation

The metabolic status of planktonic cells was evaluated 24 h after photodynamic treatment using the MTT assay. The results revealed a dose-dependent inhibition of respiratory activity by **C7** for both serotypes (Fig. 3b), as the concentration of **C7** was reduced, a gradual increase in the formazan signal was recorded, indicating a recovery of respiratory function. However, it is noteworthy that, under the tested conditions, none of the concentrations achieved the activity levels of the control without the compound (C+), even at sub-inhibitory doses.

Membrane integrity evaluation by Flow Cytometry

The cytoplasmic membrane integrity and light scattering parameters (FSC/SSC) of both serotypes were analysed following photodynamic treatment (Fig. 4a). In the untreated controls, both S4 and SB3 exhibited a population distribution shifted toward higher FSC and SSC values, consistent with the formation of bacterial micro-aggregates.

Regarding membrane integrity (SYTO-9/PI), both strains showed a dose-dependent progression toward membrane compromise (PI^+). In the untreated controls, the "live" population ($SYTO\text{-}9^+/PI^-$) predominated, with values of ~ 64.9% for S4 and ~ 69.7% for SB3. Quantitative analysis of the cytometric profiles revealed a significant decrease in the percentage of live cells and the relative live/dead ratio as the **C7** concentration increased (Fig. 4b).

Even at a sub-inhibitory concentration (1/4 MIC), a significant shift occurred, with the live cell percentage dropping drastically (to 6.01% for S4 and 4.91% for SB3) compared to untreated controls. At concentrations corresponding to the MIC and 4 MIC, the $SYTO\text{-}9^+/PI^-$ population decreased to near-undetectable levels (< 1%). These cytometric results, which characterize the membrane state at the end of the irradiation period, demonstrate a clear correlation between **C7** concentration and the loss of membrane integrity.

Activity on Salmonella spp. Biofilm

Inhibition of biofilm formation and eradication

The inhibitory capacity of **C7** against biofilm formation was assessed to determine the Biofilm Formation Prevention Concentration (BFPC). For both strains, the BFPC was established at 1.56 µM, corresponding to 1/4 of the planktonic MIC (Fig. 5a). At sub-inhibitory concentrations ranging from 1.56 to 3.12 µM, bacterial growth was detected in the planktonic phase; however, no significant adhesion to the polystyrene surface was observed. The formation of a mature and quantifiable biofilm was only observed at **C7** concentrations of 0.78 µM or lower.

The efficacy of **C7** against mature biofilms (24 h) was also evaluated (Fig. 5b). Treating established biofilms required significantly higher concentrations than those needed for planktonic cells. For strain *S.* Enteritidis S4, the Minimum Biofilm Eradication Concentration (MBEC) was determined to be 50 µM, an eightfold increase compared to the planktonic MIC. In contrast, strain *S.* Typhimurium SB3 exhibited higher recalcitrance, as total eradication was not achieved under any of the tested conditions (up to 200 µM).

Characterization of colony morphotype

The effect of photodynamic treatment on macrocolony morphology was evaluated on Congo Red agar (Fig. 5c). A **C7** concentration-dependent response was observed, with distinct phenotypic differences between the two serotypes.

For strain S4, the development of macrocolonies was completely inhibited at the MIC (6.25 µM), even when using high-density inocula (10^8 CFU/mL). At lower concentrations, this strain exhibited a reduction in total colony size compared to the untreated control. In contrast, strain SB3 maintained viability at the MIC but displayed a clear phenotypic shift from the RDAR morphotype (characteristic of the untreated control, with a complex pattern of ridges and valleys) to a PDAR morphotype. This shift was particularly evident in the 1.56 to 6.25 µM concentration range, where colonies exhibited a loss of surface striations. At the same concentrations, both strains exhibited phenotypic heterogeneity, characterized by the emergence of microcolonies within the macrocolony structure. Conversely, at the lowest concentrations tested (0.78 and 0.39 µM), both strains developed homogeneous colonies with a higher density of striations compared to the untreated control.

Quantification of Exopolysaccharides (EPS)

The production of the EPS matrix was quantified using the CR adsorption technique (Fig. 5d). The results revealed divergent profiles between the two serotypes in response to photodynamic treatment.

For *S.* Typhimurium SB3, a significant decrease in EPS production was observed as the concentration of **C7** increased from the BFPC (1.56 µM) to the MIC threshold (6.25 µM). This decrease corresponds to the phenotypic shift from the RDAR to the PDAR morphotype described previously. Conversely, at the lowest concentration tested (0.78 µM), an increase in EPS synthesis was recorded compared to the untreated control.

In contrast, *S.* Enteritidis S4 showed no significant variability in EPS production across the tested **C7** concentrations. EPS levels remained low and constant in S4, showing no significant differences compared to the untreated negative control.

Biofilm viability

To determine whether the reduction in biofilm biomass correlated with cell death, the metabolic activity of the sessile communities was evaluated using the MTT assay. The results (Fig. 5e) allowed for the identification of the viability threshold in response to photodynamic treatment. In the case of SB3, a complete absence of metabolic activity was observed at concentrations of 3.12 and 6.25 µM, indicating effective eradication of cells attempting to colonize the surface. However, at a concentration of 1.56 µM (1/4 MIC), a significant metabolic signal was detected, confirming the presence of viable cells.

This result is key when comparing the BFPC and EPS assays: at 1.56 µM, the bacteria survive the treatment but lose the ability to produce the exopolysaccharides necessary to consolidate the biofilm architecture. This suggests that aPDT, at sub-lethal doses, exerts a "disarming" effect on sessile virulence before reaching total lethality.

For strain S4, a qualitatively similar phenomenon was observed, although with significantly lower overall viability levels. Although metabolically active cells were also detected at 1.56 µM, the signal intensity was lower than that of SB3.

Discussions

The persistence of *Salmonella enterica* in the food production chain, particularly within the poultry industry, represents a formidable challenge that conventional sanitization protocols frequently fail to overcome (Mkangara 2023). This persistence is primarily attributed to the pathogen's remarkable metabolic flexibility and its capacity to form robust biofilms on diverse biotic and abiotic surfaces, which confer inherent tolerance to environmental stressors and conventional antimicrobial agents (Pang et al. 2023). This tolerance is severely exacerbated by an extracellular matrix that acts as a diffusional and protective barrier (Gentile et al. 2025), whose architectural production is closely linked to specific morphological adaptations and matrix components. The present study systematically investigated the efficacy of aPDT mediated by porphyrin derivatives against *Salmonella*, uncovering a complex, dose-dependent interplay between photodynamic stress, cellular viability, and sessile architecture. By separating the planktonic eradication dynamics from the recalcitrance of mature biofilms, our findings elucidate critical physiological and phenotypic responses that dictate the success or failure of photodynamic treatments.

A critical initial step in evaluating any antibiofilm strategy is the standardization of environmental cultivation conditions, as biofilm architecture heavily dictates the outcome of control strategies by determining antimicrobial penetration depth (dos Santos et al. 2022). Our screening of 15 *Salmonella* strains revealed that sessile biomass production is intricately dependent on the specific carbohydrate availability of the medium. We identified that a concentration corresponding to 0.25% w/v glucose in TSB, was optimal for providing the necessary metabolic balance to induce a robust sessile lifestyle and allowing 46% of the tested isolates to develop into strong biofilm formers (SBF). In stark contrast, nutrient scarcity in LBB severely limited matrix development, while higher concentrations of glucose (0.5% in TSBG) appeared to favour planktonic proliferation over sessile differentiation. This observation strongly aligns with the carbon catabolite repression (CCR) principles described by Białucha et al. (2020), where high glucose levels can trigger regulatory signals that repress cellular adherence structures. Furthermore, the temporal kinetics of biofilm formation reached a peak at 24 hours for both selected strains (S4 and SB3), followed by a progressive decrease likely driven by nutrient depletion in the static medium or the accumulation of metabolic byproducts triggering active cell dispersion as described for many bacterial strains Rumbaugh and Sauer (2020). Consequently, utilizing 0.25% glucose generates the metabolic stress required to trigger biofilm differentiation, ensuring that subsequent aPDT evaluations are conducted on optimally mature structures at their point of maximum biomass integrity.

The optimization of physical parameters for aPDT demonstrated that the initial increase in antibacterial activity, which was proportional to light exposure time, reached a statistically non-significant plateau beyond 2 hours of irradiation, corresponding to a fluence of 13.19 J/cm^2. This kinetics of saturation aligns with established photodynamic principles, where extended light exposure often triggers local oxygen depletion within the medium or induces photobleaching of the tetrapyrrolic core, rendering additional irradiation ineffective (Mokhtar et al. 2025). Therefore, 13.19 J/cm^2 was defined as the

standard light dose for all subsequent experiments, ensuring maximum photodynamic efficacy with the shortest possible exposure time.

Following the establishment of optimal parameters, our photodynamic screening identified the cationic porphyrin **C7** as the most potent photosensitizer, exhibiting a bactericidal effect with a MIC of 6.25 µM. The superior antibacterial potency of **C7** compared to its anionic counterparts (**C4** and **C5**) underscores the role of electrostatic interactions at the cell envelope. The outer membrane of *Salmonella* typically acts as a selective permeability barrier; however, the four positively charged methylpyridinium groups of **C7** could facilitate a highly efficient "self-promoted uptake" mechanism, bypassing this outer barrier through electrostatic interactions with the anionic components of the LPS (Alves et al. 2014). Upon photoactivation, this kind of photosensitizers operate primarily through highly efficient Type II photoprocesses (Austin et al. 2026). This mechanism induces severe, simultaneous oxidative damage across multiple macromolecular targets—such as membrane lipids, proteins, and nucleic acids—preventing the activation of effective cellular repair mechanisms and minimizing the risk of inducing bacterial resistance (Shariati et al. 2022), while maintaining the capacity to disrupt complex bacterial structures (Mamone et al. 2024).

The dynamics of this bactericidal effect were clearly elucidated through longitudinal survival curves. At the MIC (6.25 µM), aPDT triggered a rapid decline in bacterial viability. Immediately post-irradiation (0 h), an initial load reduction of 2.87 and 2.31 $\log_{10}$ was recorded for strains S4 and SB3, respectively. Notably, the therapeutic threshold of 3.00 $\log_{10}$ reduction—commonly considered the international benchmark for effective bactericidal activity, representing the elimination of 99.9% of the initial population—was consistently achieved by both strains at 2 hours post-irradiation. This continuous decline in viability post-exposure demonstrates an important "post-irradiation effect," where the oxidative cascades initiated during light stimulation continue to mature and damage vital cellular components even after the light source is turned off. For both strains, this state remained below the limit of detection without any signs of bacterial recovery up to 24 hours, confirming the irreversible lethality of the treatment at this concentration.

As expected, treatment with sub-lethal doses (1/4 MIC, 1.56 µM) showed cellular resilience and highlights a major methodological insight of our work regarding how different physiological assays complement each other. Following treatment at 1/4 MIC, flow cytometry profiles showed a massive and immediate migration of events toward the PI^+ quadrant, indicating widespread membrane disruption. This biophysical state closely aligns with the respiratory assessments obtained using the MTT assay, which demonstrated a significant acute decrease in metabolic viability at the same concentration immediately after irradiation. Crucially, in both evaluations, cellular damage and metabolic inhibition did not reach baseline zero; instead, a critical threshold of residual viability persisted. The survival curves provided the necessary timeline context, revealing that this small remaining, metabolically active surviving subpopulation successfully managed to initiate cellular repair pathways, driving a prominent phenotypic regrowth that restored the population within 24 hours. So, the MIC represents the critical

threshold where photodynamic stress shifts from a transient, survivable inhibition to irreversible cell death.

Beyond planktonic eradication, the true value of **C7** lies in its potent interaction with the sessile lifestyle. The biofilm formation preventive concentration (BFPC) was observed at subinhibitory concentrations of 1.56 µM (1/4 MIC), entirely abrogating surface colonization despite the presence of active planktonic proliferation in the surrounding medium. This "anti-adhesion" effect suggests that photodynamic stress fundamentally disrupts primary attachment events. Primary adhesion in *Salmonella* is mediated by specialized surface structures such as curli fimbriae and cellulose matrix components (MacKenzie et al. 2017). Based on the behaviour reported for structurally related cationic porphyrins in other bacterial models by Reynoso et al. (2019), a similar photodynamic mechanism can be hypothesized for **C7**. The high singlet oxygen yield generated by **C7** likely facilitates the direct oxidative degradation of these proteinaceous and polysaccharide components before they can anchor to the surface. Furthermore, by analogy with these related photosensitizers, the cationic nature of the porphyrin may alter the bacterial surface charge, increasing electrostatic repulsion and preventing the initial "docking" process required for biofilm initiation

This architectural interference was visually and quantitatively confirmed through macrocolony morphotypes on CR agar and EPS quantification. Upon exposure to sub-lethal **C7** concentrations, *S.* Typhimurium SB3 exhibited a phenotypic shift from the highly structured RDAR morphotype to a smoother, flatter PDAR morphotype. This phenotypic transition directly correlated with a significant quantitative decrease in EPS production within the same concentration range (1.56 to 6.25 µM). Similar to what has been demonstrated for *E. coli* (Gsponer et al. 2015), this biochemical response indicates that, under photodynamic stress, the SB3 strain would undergo an energetic "compensation," prioritizing its limited metabolic reserves towards immediate survival, maintenance of the cell envelope and intracellular repair pathways over the synthesis of the extracellular matrix, which is energetically costly. This results in a fragile, matrix-poor structure incapable of consolidating into a mature biofilm. *S.* Enteritidis S4, on the other hand, showed an absolute inhibition of macrocolony development at the MIC, and maintained a constantly low, baseline level of EPS production across all lower concentrations, confirming its inherently weaker ability to build a structured sessile architecture ("thin-matrix" biofilm) compared to SB3.

Furthermore, a lack of homogeneity will be observed in the colonies due to the appearance of distinct microcolonies within the macrocolony structure. This could be interpreted as a "risk diversification" strategy. This is a conceptual model proposed by Morawska et al. (2022) to explain how bacterial communities resist adverse environmental fluctuations. Specifically, under the selective pressure of **C7**-induced ROS, it can be proposed that the population undergoes a non-uniform physiological response. While certain cells may succumb to severe oxidative damage or enter senescence, a resilient fraction might activate protective stress-response pathways at varying rates. This type of uneven, non-homogeneous growth pattern on agar surfaces closely resembles the phenotypic heterogeneity documented by Liu and Lyu (2026) under other antimicrobial stress models. So, our macroscopic

morphological observations could reflect an adaptive community-level effort to survive sub-lethal photodynamic treatment. Conversely, at lower concentrations (0.78 and 0.39 μM), both *Salmonella* strains demonstrated a classic hormetic dose-response (Calabrese and Mattson 2017). At these sub-lethal levels, the mild oxidative stress acts as a signalling stimulus rather than a lethal agent, triggering a compensatory overproduction of matrix components that manifests as a higher density of surface striations and increased EPS synthesis, representing a defensive "over-fortification" of the colony architecture in response to perceived environmental threats.

The consequences of this architectural fortification became apparent when attempting to eradicate mature (24 h) biofilms. While aPDT effectively eliminated planktonic populations at 6.25 μM and achieved 99.9% lethality within 2 hours, mature biofilms required higher concentrations. *S.* Enteritidis S4 required a MBEC of 50 μM (an eightfold increase), while the heavily fortified *S.* Typhimurium SB3 biofilm proved entirely recalcitrant to treatment up to 200 μM. This resistance is entirely dictated by the structural complexity of the biofilm matrix. In dense, mature biofilms, the thick layer of EPS and extracellular DNA (eDNA) acts as a physical and chemical barriers that quenches and neutralizes ROS before they can diffuse into the deeper layers (Pereira et al. 2014). Furthermore, this architectural complexity limits mass transport, preventing the photosensitizer to achieve the critical concentration necessary to induce lethal damage in the basal layers of the biofilm as observed by Gsponer et al. (2015) with *E. coli*. Consequently, the persistent metabolic viability confirmed by TTC assays in SB3 reflects a fundamental limitation in light and ROS penetration rather than an intrinsic biochemical resistance of the individual bacterial cells, underscoring that biofilm architecture plays a protective role that far supersedes individual cellular robustness.

In summary, the application of **C7**-mediated aPDT presents a highly effective dual-action strategy, capable of achieving rapid planktonic eradication and targeted biofilm prevention at sub-lethal doses. However, the absolute eradication of established mature biofilms in strongly adherent, matrix-rich strains remains a formidable challenge. To overcome this structural recalcitrance, future research should be made to decipher the precise molecular targets of oxidative damage within the matrix and integrating targeted transcriptomic profiling to elucidate the immediate changes in gene expression during sub-lethal photodynamic stress, paving the way for optimized combination therapies.

Conclusions

This study demonstrates that aPDT mediated by the cationic porphyrin **C7** represents a highly efficient, dual-action strategy against *Salmonella enterica*, capable of achieving rapid planktonic eradication and targeted biofilm prevention. In planktonic cultures, **C7**-mediated aPDT at the MIC (6.25 μM) achieved the critical bactericidal threshold of a 3.00 $\log_{10}$ reduction (99.9% lethality) within 2 hours post-irradiation, confirming a robust, post-exposure toxic maturation driven by irreversible oxidative damage. Conversely, sub-lethal doses (1/4 MIC) induced only a transient inhibition, allowing for phenotypic population regrowth within 24 hours.

Regarding the sessile lifestyle, **C7** effectively established a BFPC at sub-inhibitory levels (1.56 μM), completely abrogating surface colonization. Morphotypic colony evaluations and EPS quantification biochemically validated this effect, revealing that under photodynamic stress, *Salmonella* undergoes an energetic trade-off, prioritizing immediate cell envelope maintenance and repair pathways over the synthesis of costly extracellular matrix components (driving an RDAR to PDAR transition). However, lower concentrations triggered a compensatory, hormetic matrix over-fortification, which represents a critical boundary condition to consider during the design of sanitization protocols.

Finally, the absolute recalcitrance observed in established, mature (24 h) biofilms where strain SB3 survived concentrations up to 200 μM confirms that macrocolony architectural complexity and matrix-mediated ROS quenching act as a formidable barrier to mass transport. This protective shield supersedes individual cell envelope robustness, highlighting that the elimination of mature biofilms remains a structural challenge rather than a single-cell physiological resistance. To bridge this gap, future research could integrate transcriptomic profiling to decipher immediate gene expression changes during sub-lethal photodynamic stress and exploring combination therapies capable of disrupting the matrix scaffold to exploit the full bactericidal potential of **C7**.

Declarations

Supplementary Information. Supplementary Table 1S

Acknowledgements F. Colocho wishes to thank CONICET for a doctoral grant. J. Silva is part of research support CONICET staff. C. R. Pungitore and C. S. M. Lucero-Estrada are part of CONICET researcher staff.

Author contributions Colocho Florencia Amancay: Formal Analysis, Investigation, Validation, Visualization, Writing – original draft, Writing – review & editing. **Silva Juan Eduardo:** Formal Analysis, Investigation, Validation, Visualization. **Rocca Plaza Francisca:** Investigation. **Favier Gabriela Isabel:** Funding acquisition, Resources, Supervision, Writing – review & editing. **Pungitore Carlos:** Conceptualization, Funding acquisition, Resources, Supervision, Visualization, Writing – review & editing. **Lucero Estrada Cecilia Stella Marys:** Conceptualization, Formal analysis, Funding acquisition, Resources, Validation, Visualization, Writing – original draft, Writing – review & editing.

Funding This work was supported by the Science and Technology Department, National University of San Luis, Argentina (Projects PROICO 02-1323 and PROICO 02-2620); Alexander von Humboldt Foundation, Germany, through the Linkage Program (Ref 3.4 - 1132070-ARG–IP, 2021); the National Agency for Scientific and Technological Promotion, Argentina (PICT-2021-GRF-TII-00037); and CONICET - Proyectos de Investigación Plurianuales (PIP 091).

Data availability The authors declare that the data supporting the findings of this study are available within the paper. Should any raw data files be needed in another format, they are available from the corresponding author upon reasonable request.

Competing Interest The authors declare no competing interests

References

1. Alves E, Faustino MAF, Neves MGPMS, Cunha A, Tome J, Almeida A (2014) An insight on bacterial cellular targets of photodynamic inactivation. Future Med Chem 6:141–164. https://doi.org/10.4155/FMC.13.211
2. Austin E, Wang JY, Ozog DM, Zeitouni N, Lim HW, Jagdeo J (2026) Photodynamic therapy: Overview and mechanism of action. J Am Acad Dermatol 94:1619–1632. https://doi.org/10.1016/j.jaad.2025.02.037
3. Benov L (2019) Effect of growth media on the MTT colorimetric assay in bacteria. PLoS ONE 14:e0219713. https://doi.org/10.1371/journal.pone.0219713
4. Białucha A, Gospodarek-Komkowska E, Kwiecińska-Piróg J, Skowron K (2020) Influence of Selected Factors on Biofilm Formation by *Salmonella enterica* Strains. Microorganisms 9, 43. https://doi.org/10.3390/microorganisms9010043
5. Breijyeh Z, Jubeh B, Karaman R (2020) Resistance of Gram-Negative Bacteria to Current Antibacterial Agents and Approaches to Resolve It. Molecules 25:1340. https://doi.org/10.3390/molecules25061340
6. Calabrese EJ, Mattson MP (2017) How does hormesis impact biology, toxicology, and medicine? NPJ Aging Mech Dis 3:13. https://doi.org/10.1038/s41514-017-0013-z
7. Cassidy CM, Donnelly RF, Tunney MM (2010) Effect of sub-lethal challenge with Photodynamic Antimicrobial Chemotherapy (PACT) on the antibiotic susceptibility of clinical bacterial isolates. J Photochem Photobiol B 99:62–66. https://doi.org/10.1016/j.jphotobiol.2010.02.004
8. Chen S, Feng Z, Sun H, Zhang R, Qin T, Peng D (2021) Biofilm-Formation-Related Genes *csgD* and *bcsA* Promote the Vertical Transmission of *Salmonella* Enteritidis in Chicken. Front Vet Sci 7. https://doi.org/10.3389/fvets.2020.625049
9. Di Marco N, Lucero-Estrada C, Pungitore R, C (2019) Aporphinoid alkaloids as antimicrobial agents against *Yersinia enterocolitica*. Lett Appl Microbiol 68:437–445. https://doi.org/10.1111/lam.13120
10. Di Marco NI, Iriarte HJ, Colocho FA, Maier M, Pungitore CR, Lucero-Estrada CSM (2025) Biofilm formation of *Yersinia enterocolitica* and its response against GRAS compounds in meat juice. Lett Appl Microbiol 78. https://doi.org/10.1093/lambio/ovaf112
11. dos Santos RL, Davanzo EFA, Palma JM, Castro VH, de Costa L, Dallago HMB, Perecmanis BSL, Santana S (2022) Â.P., Molecular characterization and biofilm-formation analysis of *Listeria monocytogenes*, *Salmonella spp*., and *Escherichia coli* isolated from Brazilian swine slaughterhouses. PLoS One 17, e0274636. https://doi.org/10.1371/journal.pone.0274636
12. Gentile N, Lorenzo-Rebenaque L, Marco-Fuertes A, Montoro-Dasi L, Marin C (2025) Emerging Challenges in *Salmonella* Control: The Need for Innovative and Sustainable Disinfection Strategies in Poultry Farming. Pathogens 14:912. https://doi.org/10.3390/pathogens14090912

13. Gsponer NS, Spesia MB, Durantini EN (2015) Effects of divalent cations, EDTA and chitosan on the uptake and photoinactivation of *Escherichia coli* mediated by cationic and anionic porphyrins. Photodiagnosis Photodyn Ther 12:67–75. https://doi.org/10.1016/j.pdpdt.2014.12.004
14. Liu Q, Lyu L-D (2026) Heterogeneity in microbial antibiotic responses: genetic basis and within-host evolution. Trends Genet. https://doi.org/10.1016/j.tig.2026.03.008
15. MacKenzie KD, Palmer MB, Köster WL, White AP (2017) Examining the Link between Biofilm Formation and the Ability of Pathogenic *Salmonella* Strains to Colonize Multiple Host Species. Front Vet Sci 4. https://doi.org/10.3389/fvets.2017.00138
16. Mamone L, Tomás R, Di Venosa G, Gándara L, Durantini E, Buzzola F, Casas A (2024) Laser NIR Irradiation Enhances Antimicrobial Photodynamic Inactivation of Biofilms of *Staphylococcus aureus*. Lasers Surg Med 56:783–795. https://doi.org/10.1002/lsm.23847
17. Merritt JH, Kadouri DE, O'Toole GA (2011) Growing and Analyzing Static Biofilms. Curr Protoc Microbiol 22. https://doi.org/10.1002/9780471729259.mc01b01s22
18. Methods for dilution antimicrobial susceptibility tests for bacteria that grow aerobically, 2024.. Clinical Laboratory Standards Institute
19. Mkangara M (2023) Prevention and Control of Human *Salmonella enterica* Infections: An Implication in Food Safety. Int. J. Food Sci. 2023, 1–26. https://doi.org/10.1155/2023/8899596
20. Mokhtar A, Mohamed T, Eigza AO, El-Khouly ME (2025) Water-soluble porphyrin-mediated enhanced photodynamic and chemotherapy employing doxorubicin for breast cancer. Lasers Med Sci 40:241. https://doi.org/10.1007/s10103-025-04466-z
21. Morawska LP, Hernandez-Valdes JA, Kuipers OP (2022) Diversity of bet-hedging strategies in microbial communities—Recent cases and insights. WIREs Mech Disease 14. https://doi.org/10.1002/wsbm.1544
22. Pang X, Hu X, Du X, Lv C, Yuk H-G (2023) Biofilm formation in food processing plants and novel control strategies to combat resistant biofilms: the case of *Salmonella spp*. Food Sci Biotechnol 32:1703–1718. https://doi.org/10.1007/s10068-023-01349-3
23. Pereira MA, Faustino MAF, Tomé JPC, Neves MGPMS, Tomé AC, Cavaleiro JAS, Cunha Â, Almeida A (2014) Influence of external bacterial structures on the efficiency of photodynamic inactivation by a cationic porphyrin. Photochem Photobiol Sci 13:680–690. https://doi.org/10.1039/c3pp50408e
24. Reynoso E, Ferreyra DD, Durantini EN, Spesia MB (2019) Photodynamic inactivation to prevent and disrupt *Staphylococcus aureus* biofilm under different media conditions. Photodermatol Photoimmunol Photomed 35:322–331. https://doi.org/10.1111/phpp.12477
25. Rumbaugh KP, Sauer K (2020) Biofilm dispersion. Nat Rev Microbiol 18:571–586. https://doi.org/10.1038/s41579-020-0385-0
26. Shariati A, Arshadi M, Khosrojerdi MA, Abedinzadeh M, Ganjalishahi M, Maleki A, Heidary M, Khoshnood S (2022) The resistance mechanisms of bacteria against ciprofloxacin and new approaches for enhancing the efficacy of this antibiotic. Front Public Health 10. https://doi.org/10.3389/fpubh.2022.1025633

27. Soares JM, Corrêa TQ, Barrera Patiño CP, Gonçalves IS, dos Santos GG, Guimarães GG, de Lima RV, Lima THN, Corrêa BC, Cappellini TC, de Silva Pereira S, Resende MV, de Yakovlev ALF, Blanco VV, Bagnato KC, V.S (2025) Synergistic Paradigms in Infection Control: A Review on Photodynamic Therapy as an Adjunctive Strategy to Antibiotics. ACS Infect Dis 11:2671–2691. https://doi.org/10.1021/acsinfecdis.5c00369
28. Ušjak L, Stojković D, Carević T, Milutinović V, Soković M, Niketić M, Petrović S (2024) Chemical Analysis and Investigation of Antimicrobial and Antibiofilm Activities of Prangos trifida (Apiaceae). Antibiotics 13:41. https://doi.org/10.3390/antibiotics13010041

Table 2

Table 2 is not available with this version

Figures

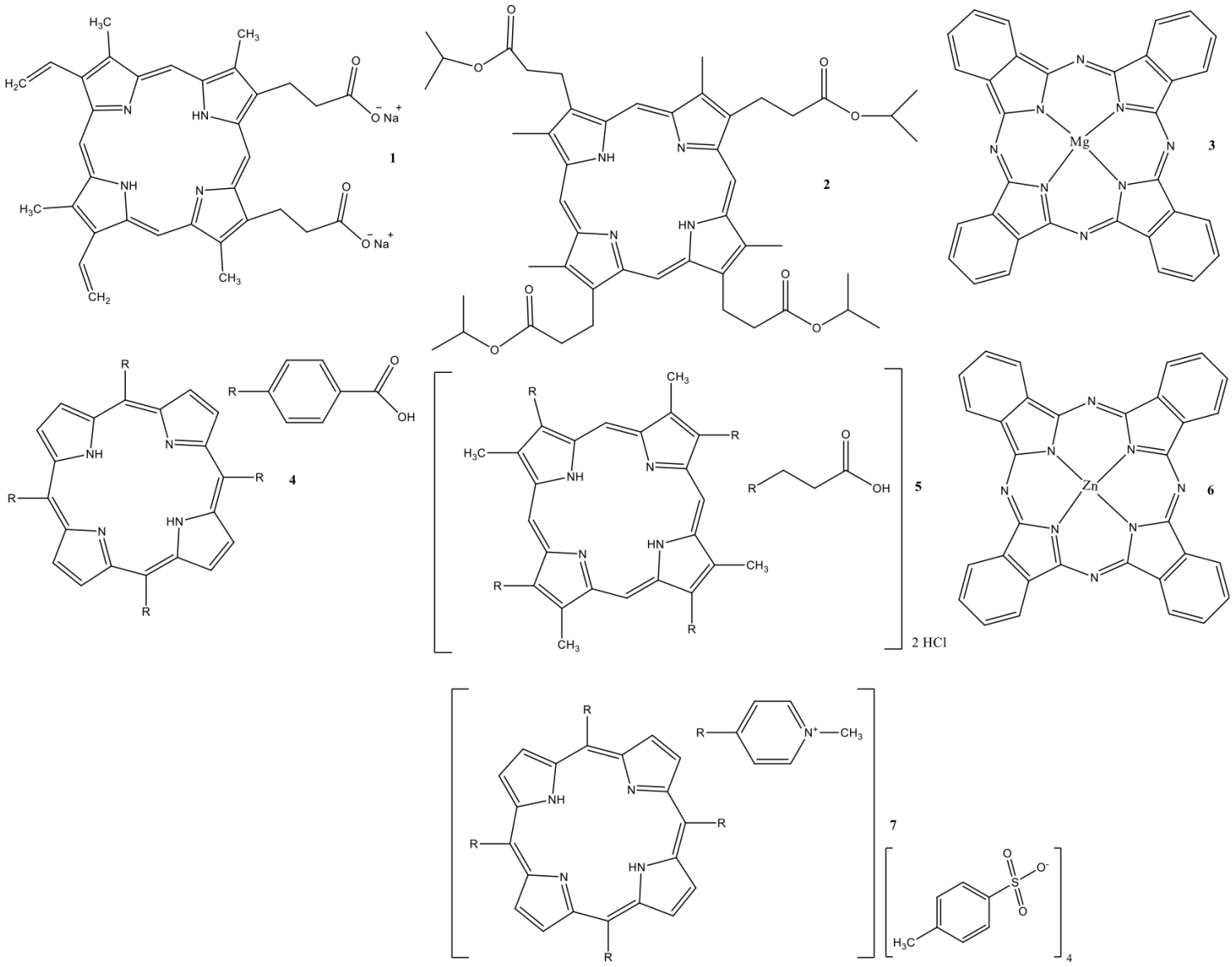


Fig. 1

Figure 1

Chemical structures of the photosensitizing agents. The panel displays the porphyrin and phthalocyanine derivatives evaluated in this study. **1**: Protoporphyrin IX disodium salt, **2**: Coproporphyrin iii tetraisopropyl ester, synthetic, **3**: Magnesium phthalocyanine, **4**: 4,4',4",4"'-(Porphine-5,10,15,20-tetrayl) tetrakis (benzoic acid), **5**: Coproporphyrin I dihydrochloride, **6**: Zinc phthalocyanine, and **7**: 5,10,15,20-Tetrakis (1-methyl-4-pyridinio)porphyrin tetra(p-toluenesulfonate).

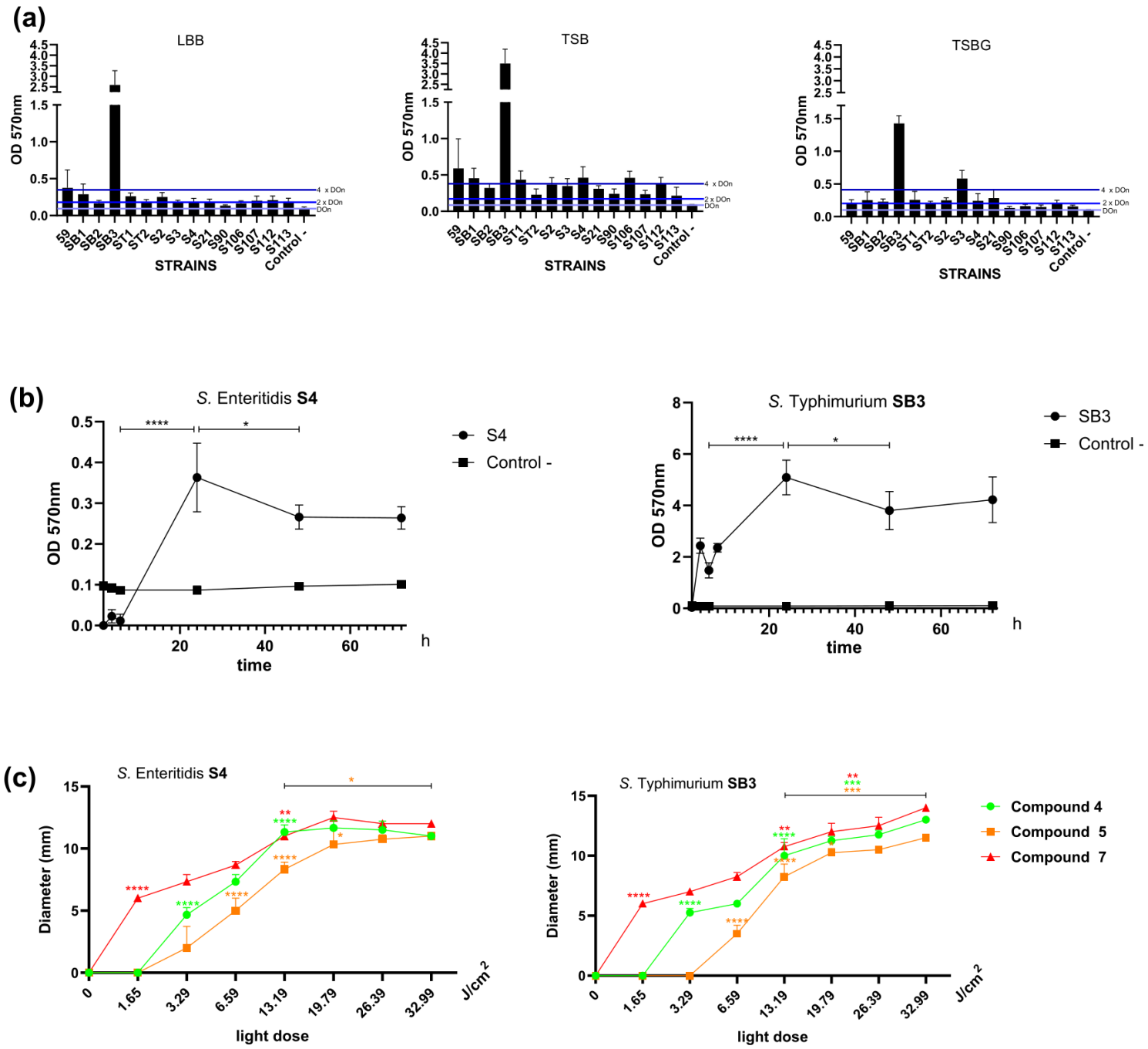


Fig. 2

Figure 2

Standardization of experimental conditions for biofilm growth and photodynamic assays. **(a)** Screening of the optimal culture medium for biofilm-forming capacity of 15 *Salmonella* strains LBB: Luria Bertani Broth, TSB Tryptic Soy Broth, and TSBG: TSB supplemented with 0.25% w/v glucose. **(b)** Biofilm growth kinetics of the selected strong biofilm formers strains monitored over 72 h in TSB to establish the optimal maturation time. **(c)**Standardization of light fluence. The effect of irradiation time on the

diameter of the growth inhibition zone was evaluated using a modified disk diffusion assay for selected compounds.

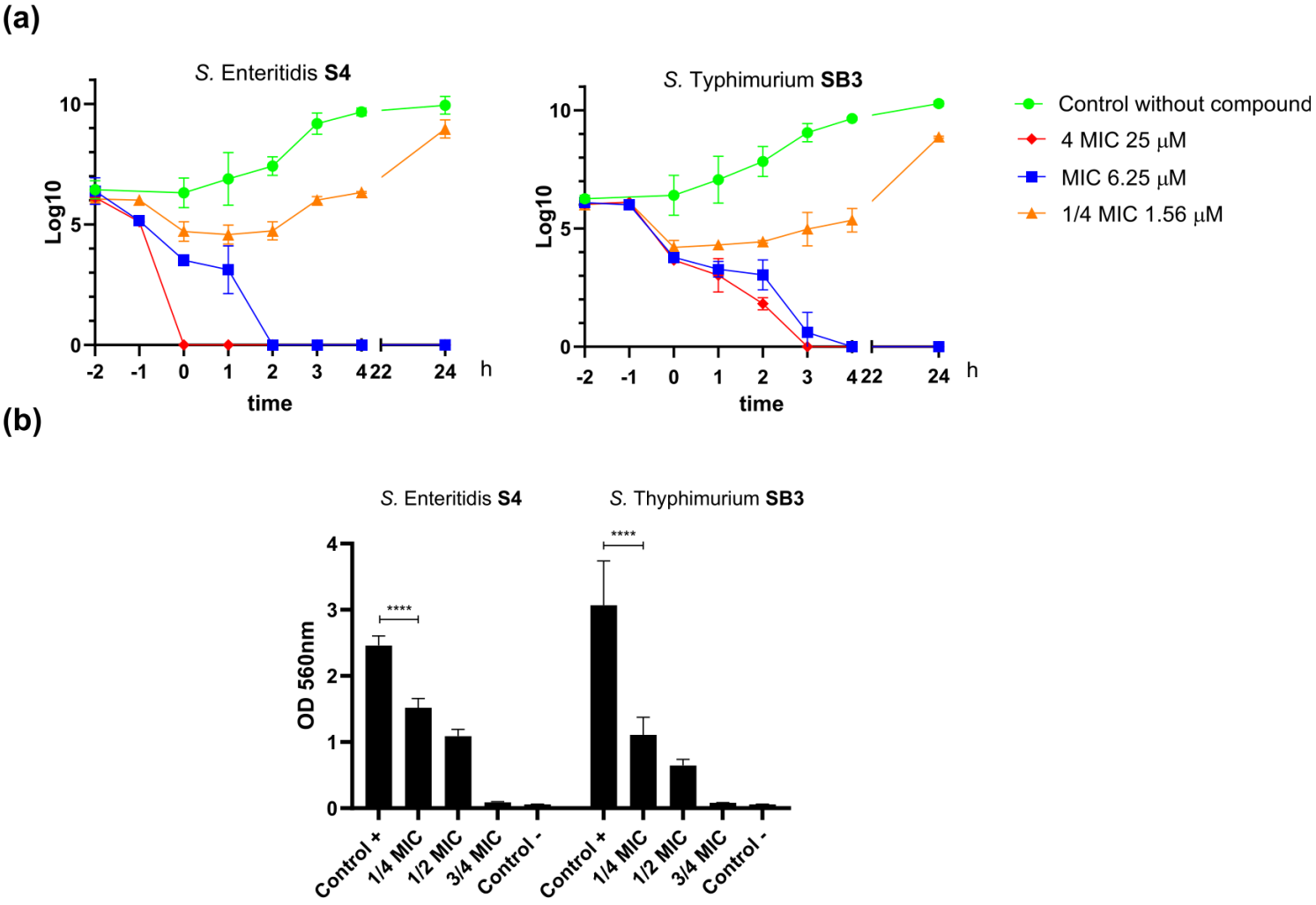


Figure 3

Antimicrobial efficacy of **C7** mediated by aPDT on *Salmonella* strains. **(a)** Survival curves of *S.* Enteritidis S4 and *S.*Typhimurium SB3 exposed to different concentrations of **C7** (¼ MIC, 1 MIC, and 4 MIC) and irradiated for 2 h. **(b)** Metabolic activity assessed by the MTT reduction assay for strains S4 and SB3. The results reflect the percentage of viable cells following photodynamic treatment relative to the untreated control.

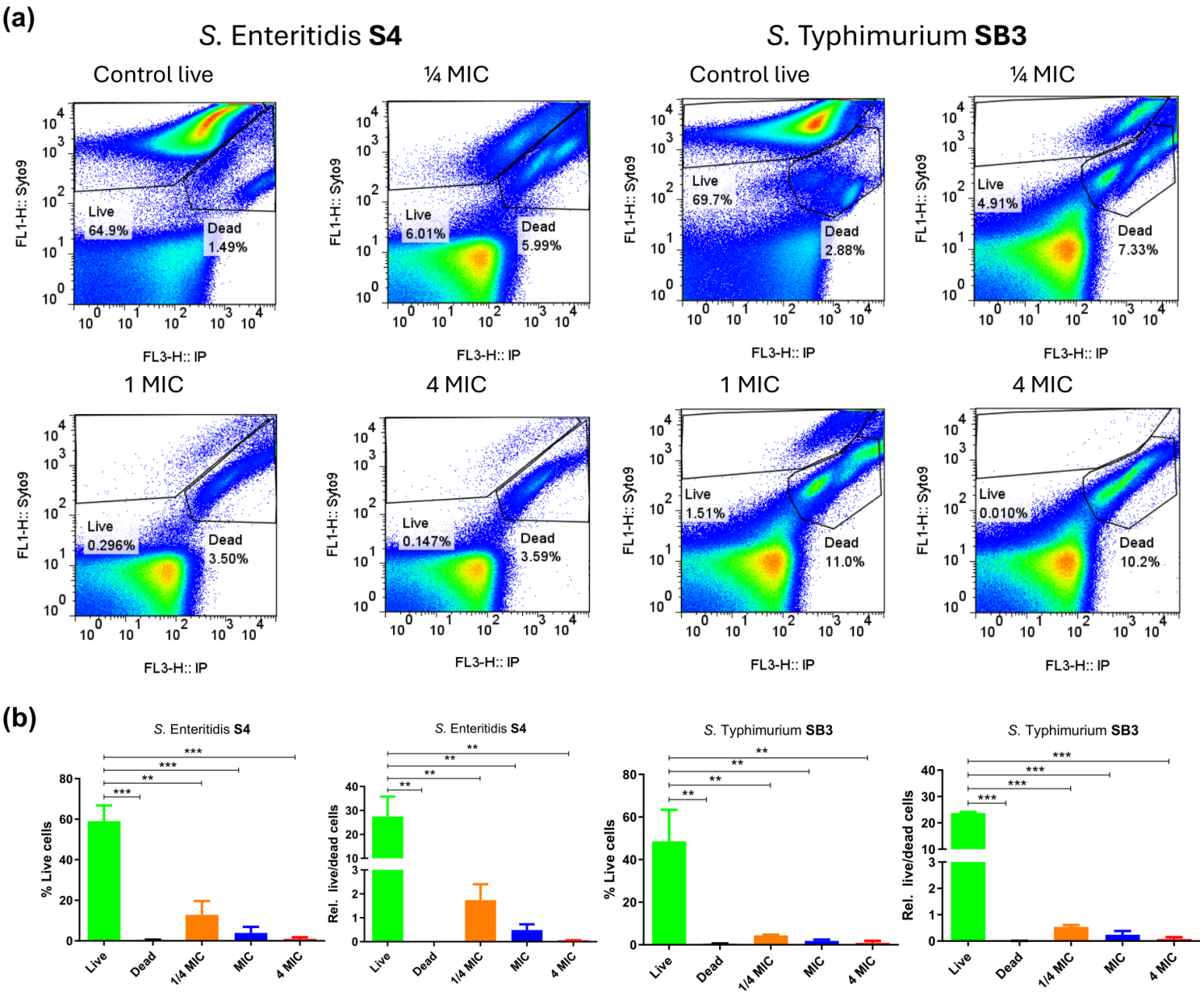


Figure 4

Physiological impact of **C7** mediated by aPDT on *Salmonella* strains. **(a)** Flow cytometry analysis of membrane integrity. Representative scatter plots (SYTO-9 vs. PI). **(b)** The graphs represent the percentage of viable cells and the live/dead cell ratio, illustrating the shift from green-stained (SYTO-9, membrane-intact) to red-stained (PI, membrane-damaged) populations as the photosensitizer concentration increases.

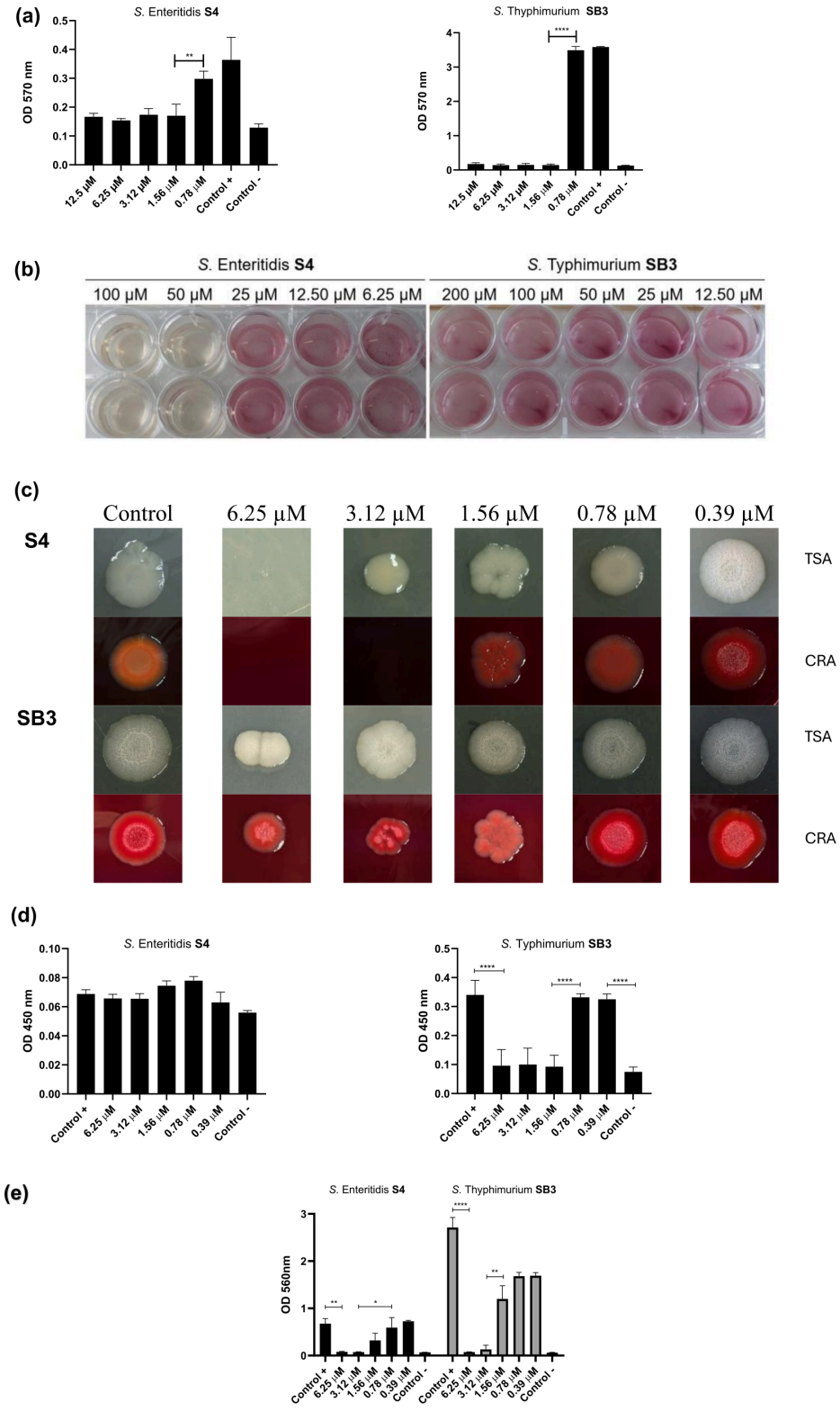


Figure 5

Impact of aPDT on *Salmonella* biofilm dynamics, architecture, and matrix composition. **(a)** Inhibitory effect of aPDT on the initial stages of biofilm formation for strains S4 (left) and SB3 (right). **(b)** Efficacy of the aPDT against mature biofilms. Fig.s show the results of one representative experiment in duplicates **(C)** Phenotypic expression of biofilm-related components (curli and cellulose) studied with macrocolony morphotypes. Representative images of macrocolonies on CRA. **(c)** Assessment of EPS

using the CR binding method. **(d)** Metabolic activity of sessile cells within the biofilm matrix measured by the MTT reduction assay. Data represent the percentage of viable sessile cells after treatment relative to the untreated biofilm control.

Supplementary Files

This is a list of supplementary files associated with this preprint. Click to download.

- graphicalabstract.png